TECHNICAL PAPER

Investigation of mechanical behavior of multi-cellular tubes with intermediate walls under lateral quasi-static loading

Wannan Guo[1]

Abstract

Energy absorbers are one of the most important structures in the automotive, shipping and aerospace industries. These structures are made in two types: reversible and irreversible. In this study, thin-walled irreversible energy absorbers were investigated. These absorbers are a new type of multi-cellular structure consisting of several concentric cylinders and two perpendicular walls, and their mechanical behavior and collapse properties have been studied under quasi-static lateral loading. The present study has been done by experiments and simulations. For simulations, LS-DYNA was used and three different groups of absorbers were simulated, including mono-cylindrical, bi-cylindrical (C2) and tri-cylindrical. According to the results obtained from the force–displacement curves, it was found that increasing the thickness in each of the components, including the walls and cylindrical shells, leads to increasing the mechanical properties such as specific energy absorption, maximum force and crushing force efficiency. Also, a comprehensive analysis was performed on the force–displacement curves of these structures. It was observed that for each group of absorbers, the collapse of each wall causes peak force s in the force curve. It was also observed that in Group C2 absorbers, the collapse of the cylinders had a more uniform force curve compared to the collapse of the walls, and the greater the thickness of the cylinders and the smaller the thickness of the walls, the smaller the difference between the uniform part and the peak force.

Keywords Energy absorber · Multicellular structures · Specific energy · Crushing force efficiency · SEA

1 Introduction and background of research

Thin-walled energy absorbers are one of the structures used in car bodies as a safety system [1]. This structure prevents collisions with the passengers during traffic accidents by converting the kinetic energy of the cars into plastic deformations that occur in the absorber body [2]. So far, different types of energy absorbers have been introduced. In the past, these absorbers were made using metal materials such as aluminum and steel, but today, due to advances in technology and materials, the number of manufacturing methods and materials used in energy absorbers is increasing every day. Fiberglass-reinforced composite materials [3, 4] as well as filaments used in 3D printers such as PLA [5, 6] and ABS

[7, 8] are among the new materials that have been recently introduced. Researchers around the world are trying to identify the absorbers that work best for them. Among these, the performance of energy absorbers can be evaluated by examining several parameters. These parameters are mainly obtained from force–displacement curves. Thus, each energy absorber has a curve during its collapse process, according to which the performance indicators of the absorber can be extracted. One of the most important indicators of any energy absorber is the area below the force–displacement diagram, which shows the energy absorbed in the absorber (Energy or EA) [9]. Another indicator that is important in any force–displacement curve is the initial peak force. This force mainly represents the maximum force in the curve (Fm) [9]. By dividing the energy absorbed in the absorber by the mass of the absorber and the length of the absorber collapse, the specific energy absorption (SEA) [9] and the average force (Fa) [10] are obtained, respectively. It should be noted that by dividing the average force by the maximum force, the crush force efficiency (CFE) [10] is obtained. Research in the field of energy absorbers is often done in

✉ Wannan Guo
  guown524@126.com

1   School of Mechanics and Engineering, Liaoning Technical University, Fuxin 12300, China

both quasi-static and dynamic forms. The following are some of the studies that have examined energy absorbers.

Wang et al. [11] investigated the energy absorption of sandwich panels containing intersecting circular sections with triangular cores under lateral loading. In their

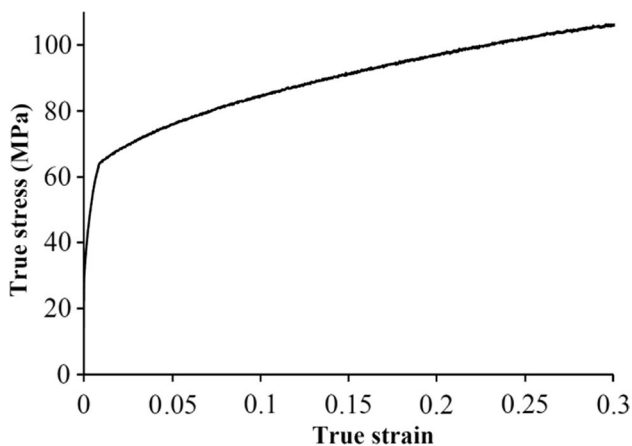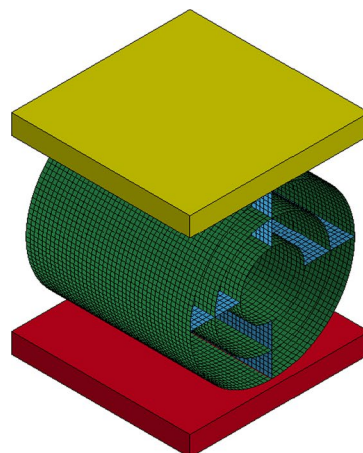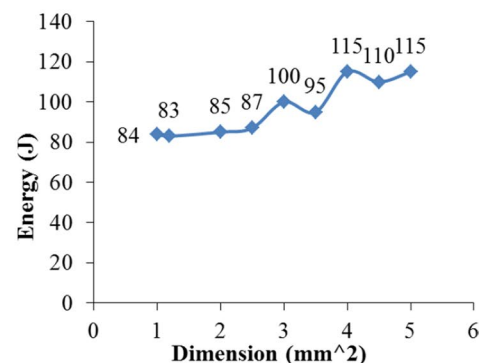**Fig. 1** Samples prepared for experimental studies

Fig. 2 True stress–strain curve for 6063 aluminum

research, they used LS-DYNA software for simulation, and good agreement between experimental and numerical results was observed. In a study conducted in 2019 by Usta and Türkmen [12] on nested absorbers, the effect of adding ABSplus honeycomb cells on the collapse behavior of nested absorbers was investigated, their specimens were investigated under impact loading. It was revealed that using honeycomb as filler has a high influence on the crushing properties of single and nested tubular structures. In a 2019 study, Yang et al. [13] investigated elliptical cross-sectional absorbers analytically, experimentally, and numerically. In their analytical studies, they used a rigid-perfectly plastic material model. Fourfold-tube absorbers were introduced by Wang and Xu [14]. Their absorbers were tested under lateral quasi-static loading numerically and experimentally. LS-DYNA was used for simulation; the results showed that the fourfold-tube system (FT) can show the most efficient impact force. Nested tube structures with rectangular cross sections were investigated by Tran [15]. He did his article in both experimental and analytical methods. In his analytical investigation simple superposition principle was used. Baroutaji et al. [16–18] introduced different arrangements of nested tubes under lateral loading. Dynamic and quasi static tests were done in their investigations. Their works could be a good reference for lateral loading of nested tubes. Alavi Nia et al. [10, 19, 20] investigated nested multi-tubular absorbers under axial quasi static loading. In their works, they proposed different heights for their tubes which leads to lower maximum force. They optimized their structures based on RSM method. Elahi et al. [21] studied foam-filled absorbers under lateral loading. Their proposed theoretical model was based on Castigliano's theorem. Chahardoli et al. [22, 23] investigated different types of nested energy absorbers under axial quasi-static loading. They used LS-DYNA in their simulations and showed that combining different circular and rectangular shells leads to better performance under axial and lateral loading. Tang et al. [24] studied the

Fig. 3 A: Finite element model simulated in LS-DYNA, B: Mesh convergence study for C111

A

B

crushing properties of multicellular columns under axial impact loading. They investigated the effects of geometrical parameters on collapse properties, and it was revealed that thickness of wall, and also the number of cells along the radial and circumferential directions have a significant effect on absorbed energy. In another study which was done by Xiong Zhang and Hui Zhang [25], axial collapse of circular multi-cell columns was investigated experimentally and numerically under impact loading.
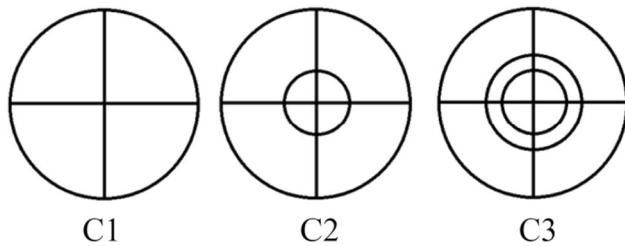

Fig. 4 General geometry of the simulated samples

Given the history of energy absorbers, these structures are constantly being reviewed and updated. Since the issue of motor vehicle accidents has always been considered by researchers to reduce the damage caused by traffic accidents, the topic of energy absorption was chosen for further study. In this study, a new type of multi-cellular absorber has been proposed. These absorbers consist of 4 walls and a maximum of 3 concentric cylinders, which are more efficient than single cylinders that are subjected to quasi-static loading. Investigated absorbers of this manuscript have not been studied in previous studies. Also their force–displacement diagrams are compared in more detail and based on initial loads.

2 Raw materials

The raw materials required for this research are 6063 aluminum cylinders. Figure 1 shows the cylinders intended for experimental tests. Three different types of cylinders with diameters of 83, 58 and 32 mm were prepared, the thickness of the large, medium and small cylinders were 2, 2.1 and

Table 1 Decomposition characteristics of simulated samples under quasi-static lateral loading

Code	Energy (J)	mass (g)	SEA (J/g)	Fm (KN)	Fa (KN)	CFE (%)
C111	85	94	0.9	6.3	1.2	19
C112	247	152	1.63	8.1	3.5	44
C113	484	210	2.31	11.2	6.9	62
C121	214	131	1.63	13.6	3.1	22
C122	442	189	2.34	15.2	6.3	42
C123	745	247	3.02	17	10.6	63
C131	428	168	2.55	21	6.1	29
C132	705	226	3.12	22.8	10.1	44
C133	1093	284	3.85	25	15.6	62
C211	101	103	0.98	7	1.4	21
C212	301	183	1.64	10.1	4.3	43
C213	757	263	2.88	19.3	10.8	56
C221	207	125	1.66	13.5	3	22
C222	435	205	2.12	16.4	6.2	38
C223	884	285	3.1	23.4	12.6	54
C231	301	148	2.04	19.7	4.3	22
C232	671	228	2.94	26.5	9.6	36
C233	1101	308	3.57	33.8	15.7	47
C311	185	143	1.29	7.5	2.6	35
C312	523	263	1.99	18.4	7.5	41
C313	893	384	2.33	23.7	12.8	54
C321	272	166	1.64	13.9	3.9	28
C322	700	286	2.45	22.8	10	44
C323	1281	406	3.15	40.8	18.3	45
C331	356	188	1.89	20.4	5.1	25
C332	920	308	2.99	29.8	13.1	44
C333	1535	429	3.58	48.5	21.9	45

1.1 mm, respectively, and their length was 83 mm. In order to ensure the validation of the tests, a replication of each sample was prepared. Figure 2 shows the true stress–strain curve for all three samples. To extract the stress–strain curve, dumbbell-shaped samples were extracted based on the dimensions presented in the reference [26] and were subjected to tensile testing in the machine. It must be noted that the approximate yield stress for Al6063 is around 150 MPa, in this investigation, in order to have a similar stress–strain curve for tubes they were annealed (they were subjected to a temperature of 420 °C for 2 h and then their temperature were decreased in room temperature).

3 Numerical simulation

In order to simulate the proposed absorbers in this research, LS-DYNA finite element software was selected. Although LS-DYNA is appropriate for Impact problems but in may many studies it was used for quasi static loading [27, 28]. According to the model shown in Fig. 3A which is a finite element model of simulated absorber, to model the elements related to walls and pipes, a shell element with 2 * 2 mm dimensions was used. Selecting this dimension was based on a mesh convergence study which is presented in Fig. 3B; this figure shows the amounts of absorbed energy for a specimen with a code of C111 which would be introduced in the following paragraphs. As it can be seen after dimension of 2×2 mm^2 the amount of absorbed energy doesn't change significantly. Mat-piecewise-linear-plasticity material model was used to introduce the mechanical properties of aluminum to LS-DYNA. The required properties for this model were loaded into the software according to the

stress–strain diagram of Fig. 2, which is for 6063 aluminum. The Young's modulus of aluminum is 70 GPa and the yield stress for the stress–strain curve shown in Fig. 2 is 43 MPa.

The simulated absorbers were placed between the upper and lower jaws as shown in Fig. 3. The lower jaw is fixed and the upper jaw moves downward in a quasi-static manner until

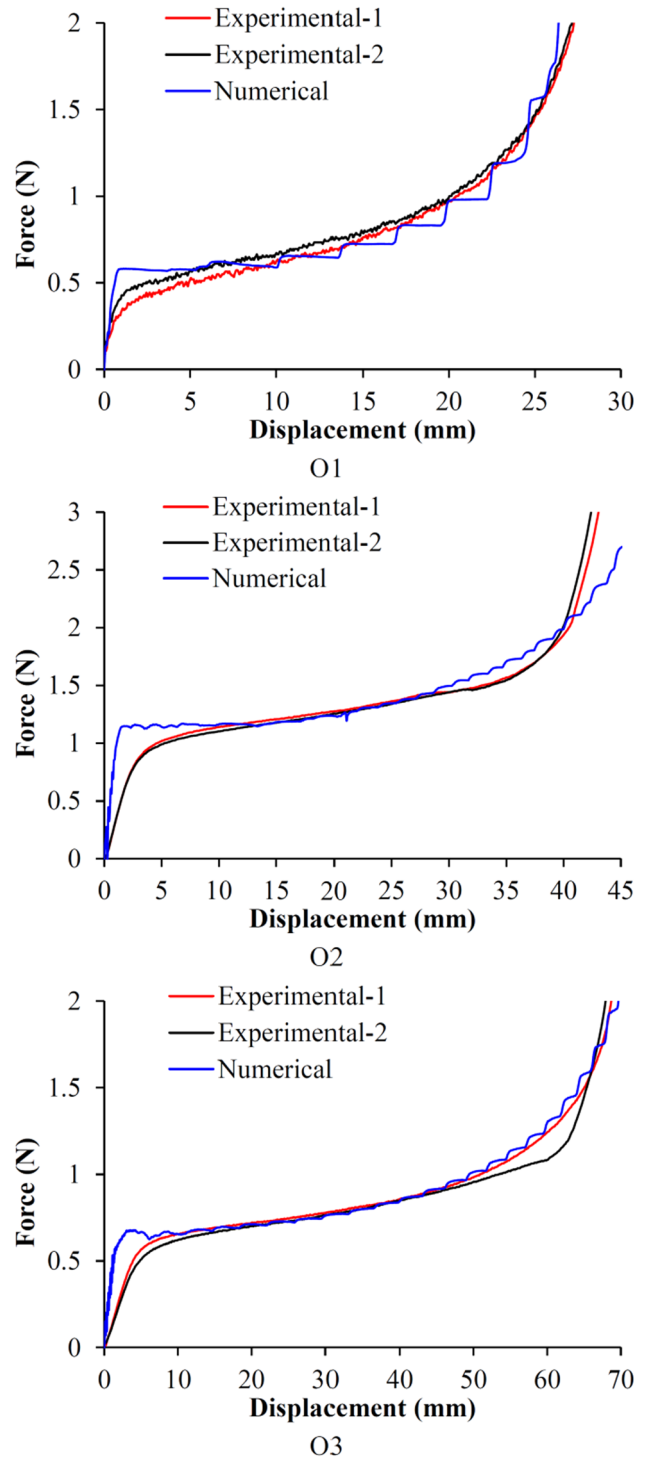**Fig. 5** How to place the samples between the jaws of the device

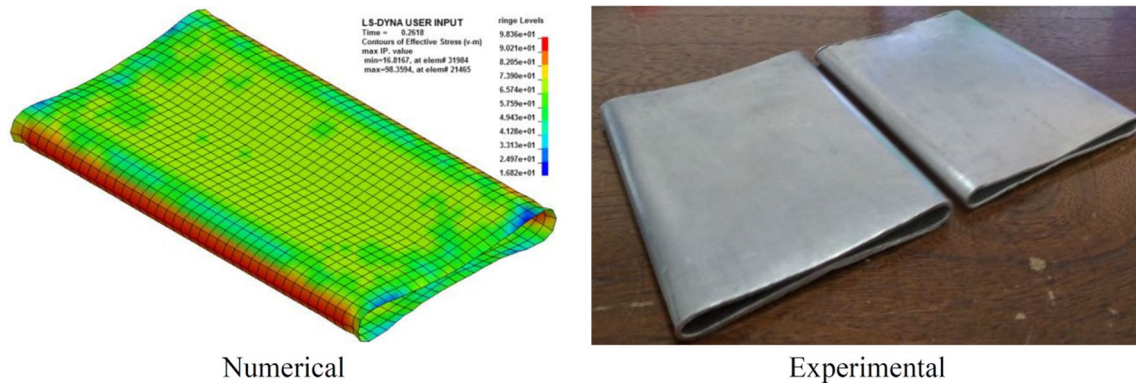**Fig. 6** Force–displacement curves for validation of numerical results

Fig. 7 Comparison of the collapsed state of the O1 sample in experimental tests and numerical simulations
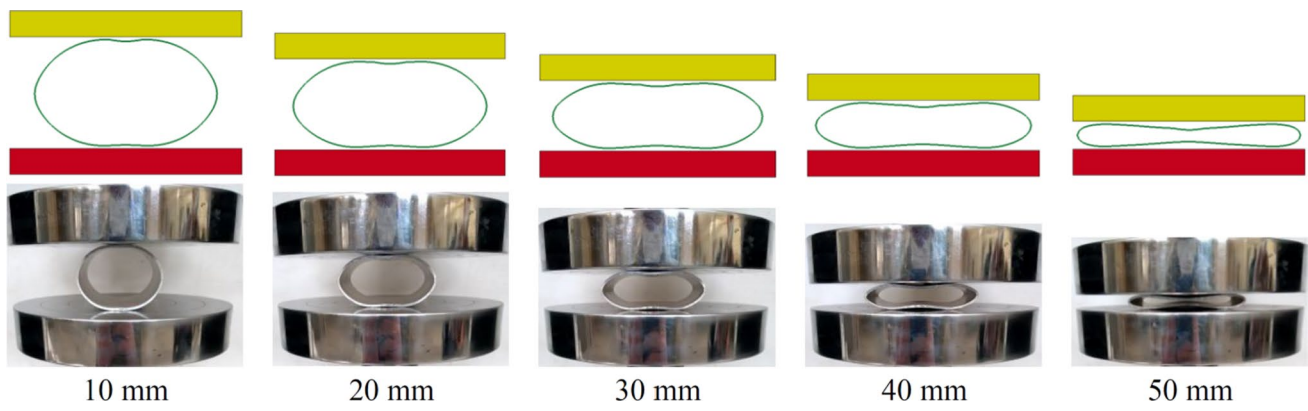

Fig. 8 Comparison of collapse stages of O2 sample in experimental and numerical cases

the absorber completely collapses. The coefficients used to define static and dynamic friction were selected to be 0.3 and 0.2, respectively.

In this section, 27 different examples are simulated. In terms of the number of inner cylinders, these specimens can be divided into three different categories, the lateral cross-sectional geometry of which is shown in Fig. 4. Among these three categories, the diameters of large, medium and small cylinders were 83, 58 and 32 mm, respectively. It should be noted that the length of all three cylinders, like the experimental samples in Fig. 2, was equal to 83 mm.

In each of the geometries presented in Fig. 4, three thicknesses of 1, 2 and 3 mm were considered for all walls and three thicknesses of 1, 2 and 3 for all cylinders. In naming the simulated samples, the initial letter and the number after it represent one of the geometries presented in Fig. 4, and the numbers that come after these geometries, show the wall thickness and the thickness of the cylinders in millimeters, respectively. For example, C231 represents an absorber that has the geometry of C2 and has a thickness of all its walls of 3 mm and a thickness of all its cylinders of 1 mm. Table 1 shows the collapse characteristics of all simulated samples.
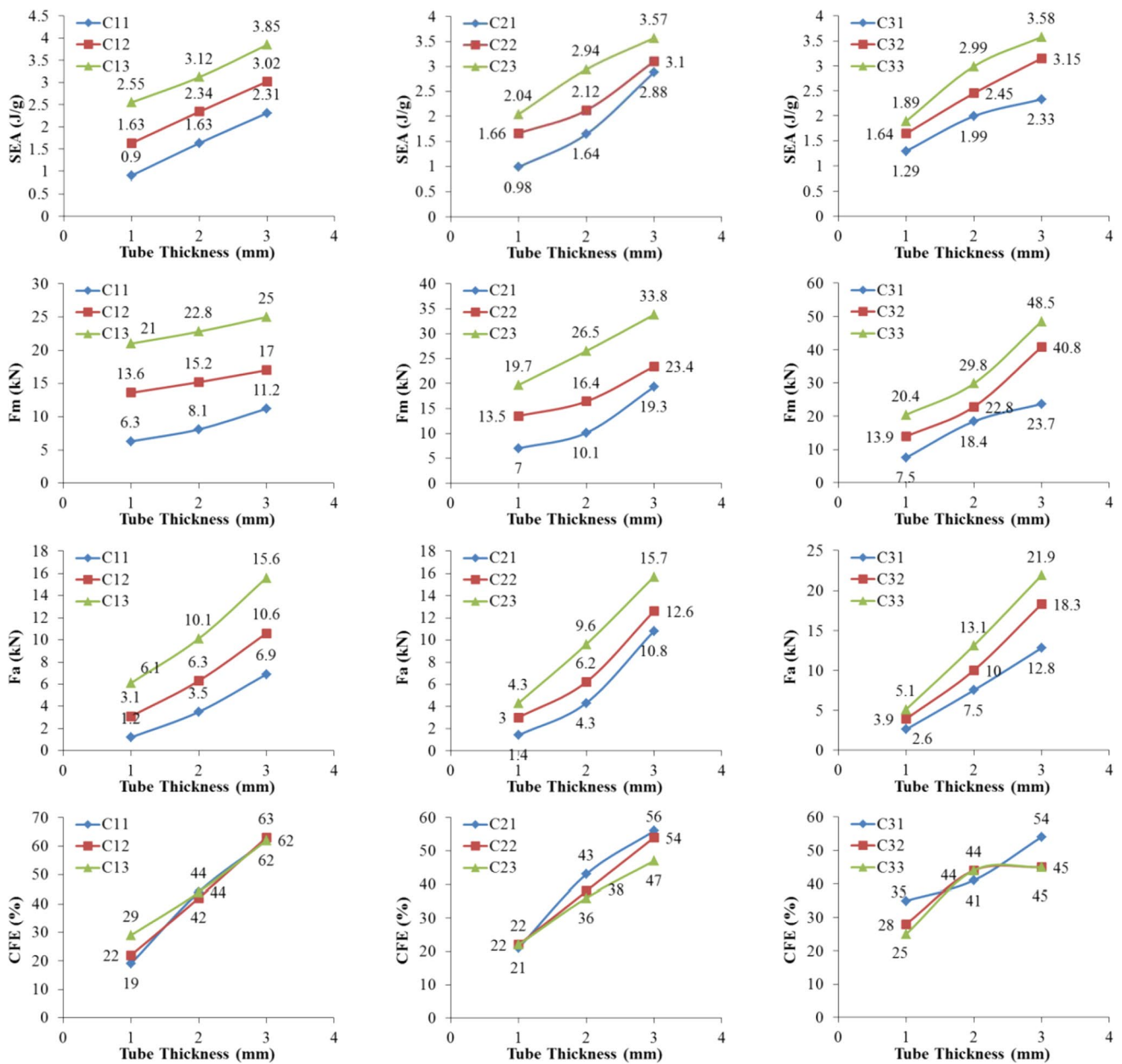
Fig. 9 Comparison of collapse properties of simulated samples

3.1 Validation of numerical simulations

In order to validate the simulations, the samples prepared in Sect. 2 were subjected to quasi-static compression tests. Figure 5 shows how these samples were placed between the jaws of the device. Figure 6 shows the force–displacement curves of these specimens under quasi-static lateral collapse,

which is both experimental and numerical. The letters O1, O2, and O3 represent specimens with small, medium, and large diameters. Figure 7 compares the collapsed shell of the O1 sample in experimental and numerical modes. The collapse stages of the O1 sample are also shown in Fig. 8.

Considering Fig. 6 shows that the initial slope of the force curve in the simulation mode is greater than in the
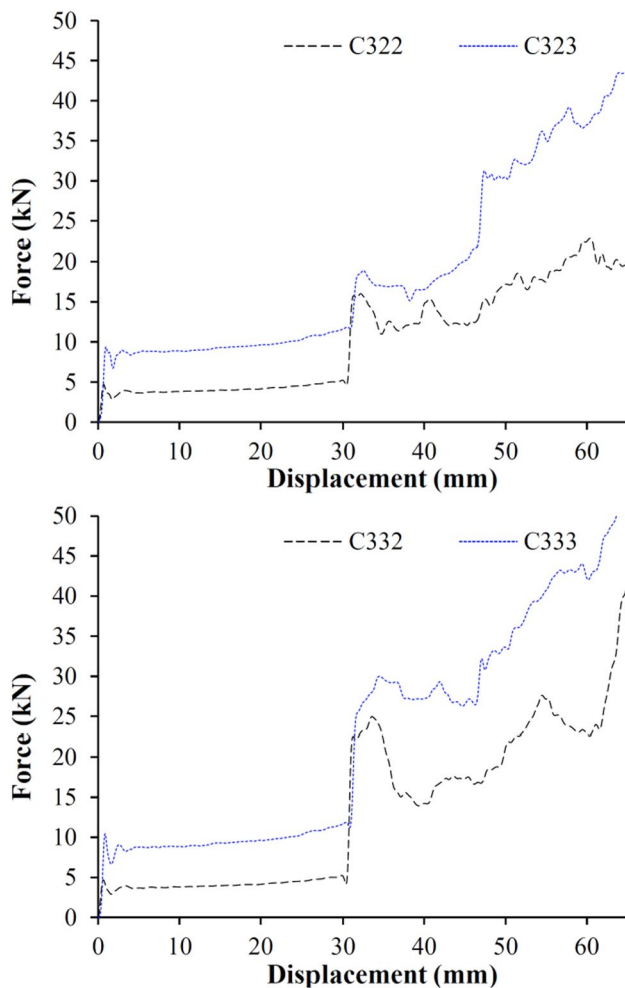
Fig. 10 Comparison of force–displacement curves for C322 and C323 samples as well as C332 and C333 samples

experimental case. This is due to the completeness and uniformity of the thickness of the samples in numerical case. Also, in numerical mode, there is no distortion in the samples, and therefore, it is expected that all samples in numerical case have more initial force. A comparison of the area below the graph for the experimental and numerical cases shows that the same level is obtained for both cases, and this indicates that in both cases the samples absorb the same energy. Based on the comparison between the experimental

and numerical results, it can be seen that LS-DYNA software can make accurate predictions about force–displacement curves, collapse states, and collapse parameters. Therefore, the results obtained in Table 1 can be analyzed with good confidence.

4 Results and discussion

In this part of the research, the collapse characteristics for the results obtained in Table 1 are investigated.

4.1 Investigation of the effect of wall and circle thickness on the collapse characteristics

As mentioned in the previous sections. In each instance, the number 2 at the end of each code indicates the thickness of the circular cylinders, which can be 1, 2, or 3. As can be seen, Fig. 9 indicates changes in the collapse characteristics in terms of changes in the thickness of the shells and walls (based on data presented in Table 1). According to these figures, it is clear that increasing the tube thickness leads to an increase in the collapse properties, also comparing absorbers in different groups shows that absorbers with higher wall thickness have higher amounts of collapse properties. Among the studied characteristics, increase in specific energy and crushing force efficiency are positive changes and indicate improvement in the collapse properties, but increase in maximum force is a negative change and should be avoided as much as possible.

4.2 Investigation of force–displacement curves and collapse states

According to Fig. 9, regarding the crushing force efficiency for the samples in groups C32 and C33, it can be seen that in these samples, the increase in the thickness of the cylinders from 2 to 3 did not create significant changes in the crushing force efficiency. To investigate this issue, the force–displacement curves for C322 and C323, as well as C332 and C333, are shown in Fig. 10. According to these two curves, it can be seen that although the average collapse force (Fa) for both C323 and C333 samples increased compared to C322 and

Fig. 11 A: Force–displacement curve for Group C1 specimens, B: Initial part of the force–displacement diagrams for Group C1 specimens
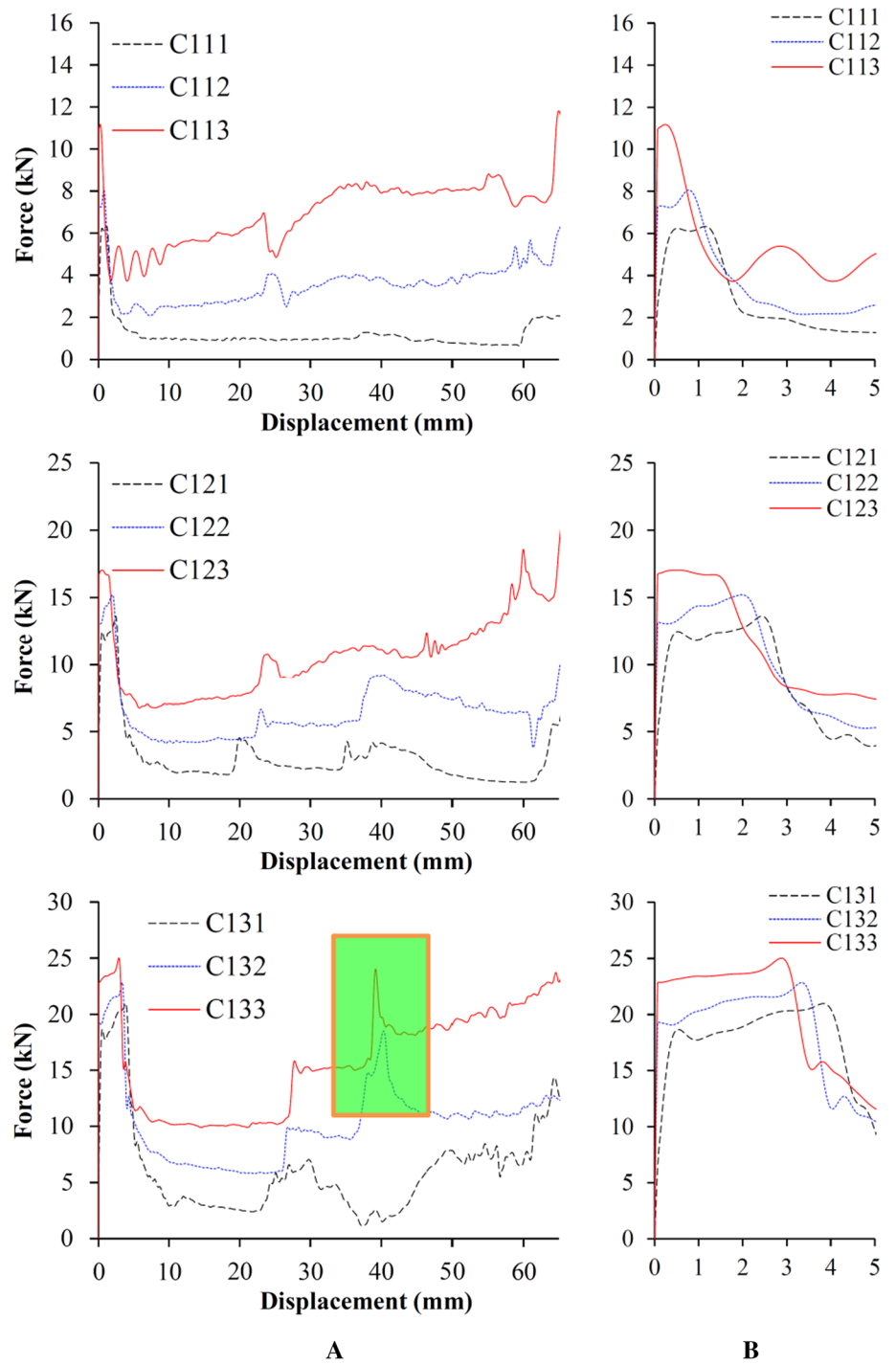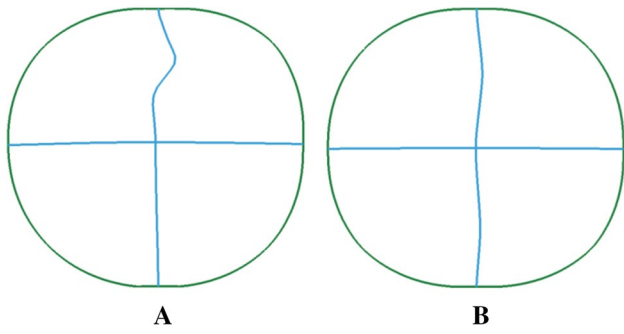
Fig. 12 A: Early stage of collapse of samples C111, C112, C113 and C21, C122, C123 and samples C132 and C133 B: Early stage of collapse of samples C131

C332 samples, but the maximum force also increased and the same increase in maximum force prevents the increase of CFE according to the definition of crushing force efficiency.

Reviewing Fig. 10 shows that in the process of collapse of the samples shown, there are sudden changes in the force–displacement curves. To further investigate this change, the force–displacement curves of all samples are given in the following sections.

Examining the diagrams in Fig. 11A, it can be seen that in these diagrams the initial maximum force occurred at the beginning of the collapse process. This maximum force can occur due to the collapse of the wall or the collapse of one of the cylinders that make up the structure. Figure 12 shows the first collapse stage for all C1 group samples. As can be seen in this figure, the collapse of all C1 group specimens occurred by buckling the upper part of the vertical wall. However, in C131 samples, wall collapse occurred at both the top and bottom. The higher wall thickness compared to cylinder thickness increases the probability of simultaneous collapse of both the upper and lower parts. A closer look at the force–displacement curves of Fig. 11A shows that in Group C1 specimens, the maximum force stability increases with increasing wall thickness from 1 to 3. To better understand this issue, the beginning of the force–displacement diagrams is shown in Fig. 11B. Figure 6, which is related to the lateral collapse of cylindrical shells, shows that these shells do not have any sudden increase in their force curve, and since increasing the wall thickness makes it stronger, so collapse at the beginning of the process for those specimens
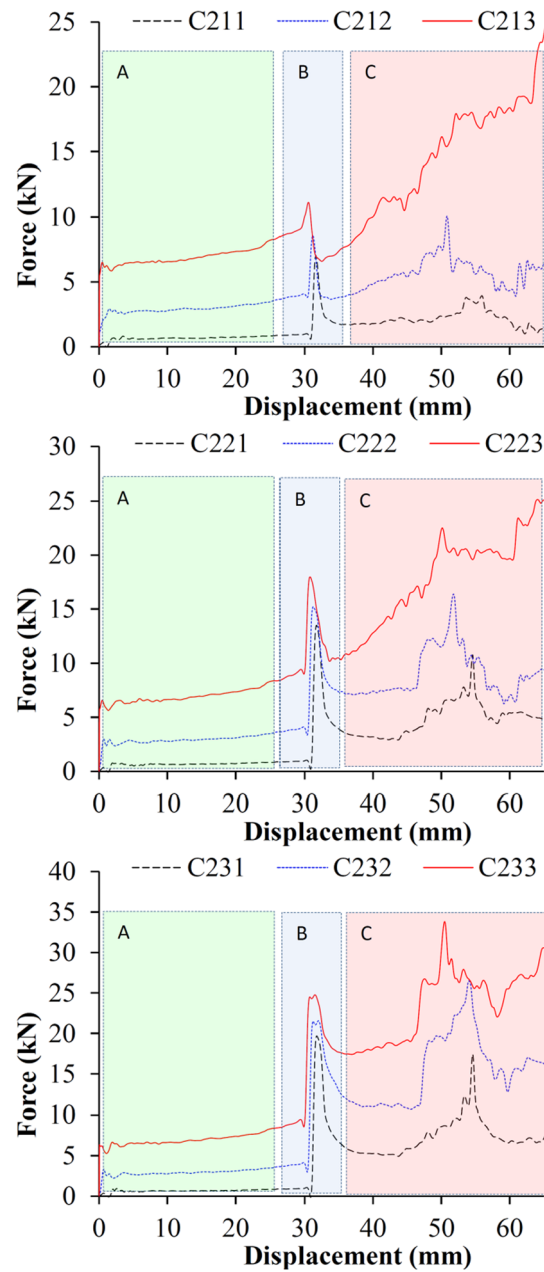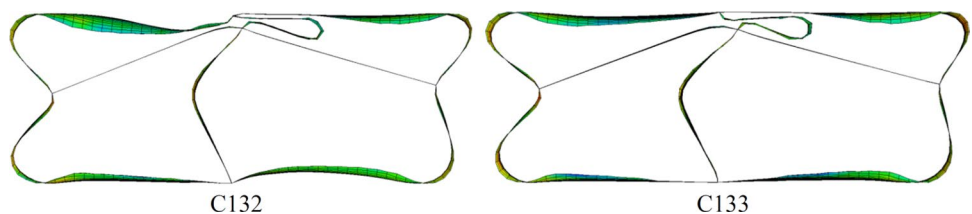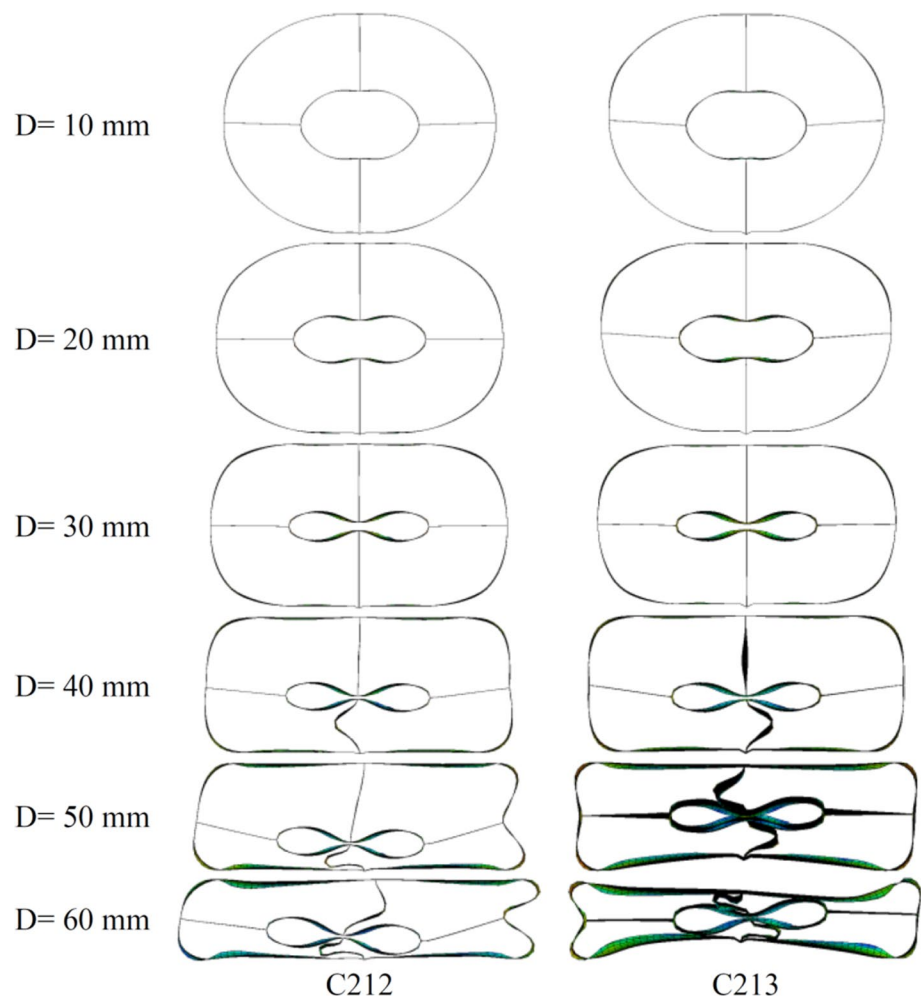

Fig. 14 Force–displacement curve for Group C2 samples

with a wall thickness of 3 mm is in the form of a combined collapse which involves the simultaneous collapse of both

Fig. 13 Bending of the lower part of the vertical wall for samples C132 and C133

Fig. 15 Decomposition steps for samples C212 and C213

parts of the vertical wall (top and bottom) and the cylindrical shell.

It should also be noted that often a sudden increase in the force–displacement diagram is due to the sudden collapse of the wall. Looking at the highlighted area shown in Fig. 11A, shows that the force curves of the C132 and C133 specimens have a sudden peak at the end of their collapse process. This peak is due to the sudden collapse of the lower part of the vertical wall. Figure 13 shows the buckling of the lower part of the vertical wall for both specimens.

Figure 14 shows the force–displacement curves for the C2 group samples. A distinctive feature of the force diagrams of these specimens is the presence of a peak force at a displacement of 30 mm. As can be seen in this figure, the curve can be divided into three different parts. In the initial part of the diagram, the force curve is almost uniform, in the middle part there is a sudden jump in the curve, and in the final part, while the force gradually increases, a secondary peak force occurs in the curve.

To justify the behavior of the curve in the C2 samples, it is useful to refer to the collapse pattern of these samples.

Figure 15 shows the collapse steps for samples C212 and C213. As shown in Fig. 15, at displacements between 0 and 30 mm, the collapse of the absorbers is mainly due to the collapse of the cylinders, and in this collapse there is no deformation in the walls, but as the collapse progresses. At displacements of nearly 30 mm, the lower vertical wall collapses and the force curves experience their first peak. After a displacement of 30 mm, the collapse of the structure continues with the deformation of the cylinders and walls (except the upper wall). Then the upper wall buckles at the displacement of 50 mm and the curve experiences the second peak force. Another point that can be deduced from the diagrams in Fig. 14 is that at a constant thickness for the walls, the greater the thickness of the cylinders, the smaller the difference between the peak force of zone B and the uniform force of zone A.

Figure 16 shows the force curves of the C3 group samples. As can be seen in these diagrams, the force curves have a significant peak force at a displacement of 30 mm. The reason for this sudden increase was explained in the previous paragraphs. It should also be noted that the diameter of the innermost cylinder is 32 mm and in all samples with more than two cylinders (groups C2 and C3) after the collapse of the innermost cylinder, the first peak of force with buckling of one of the vertical walls occur.

Among the diagrams in Fig. 16, the curve for the C313 sample is slightly different from the other curves. In this curve, the force diagram experiences an initial peak at the beginning of the collapse process. This is due to the fact that the cylindrical shells become more resistant with increasing thickness, so that in samples where the thickness of the cylinders is high, the displacement of the upper jaw cannot cause acceptable deformation in the structure of the cylinder and therefore the buckling of a 1 mm thick wall begins in the very early stages of collapse. Figure 17 shows the collapsed state of all specimens at a displacement of 60 mm. As can be seen in this figure, in all specimens except the C313 specimen, the inner cylinder has completely collapsed at a displacement of 60 mm.
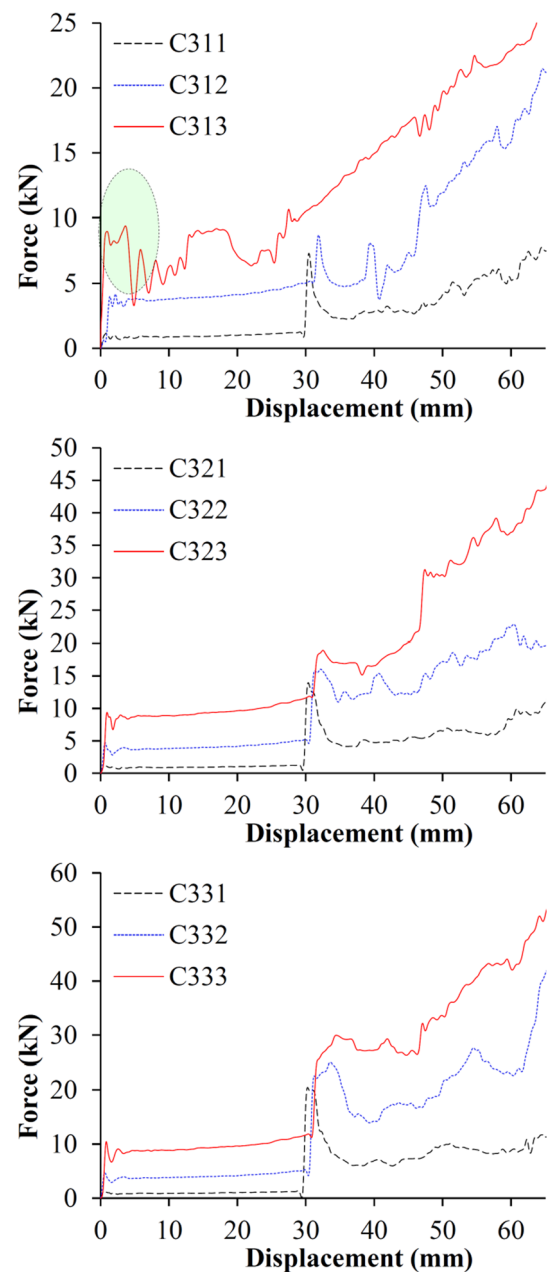

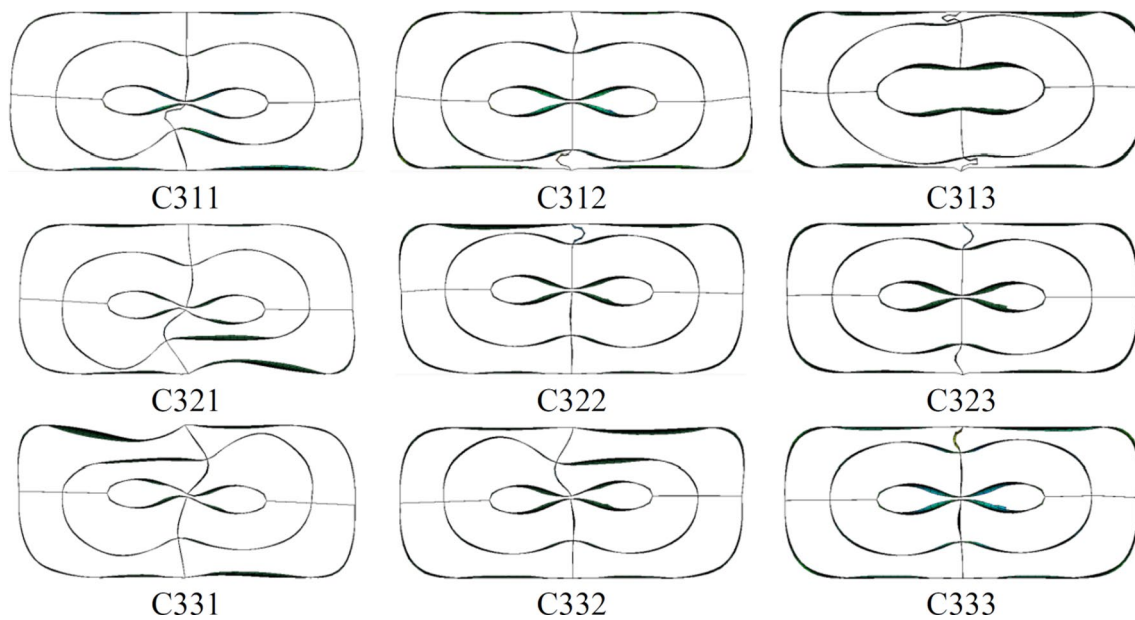**Fig. 16** Force–displacement curve for Group C3 specimens

Fig. 17 Collapse of Group C3 specimens at a displacement of 60 mm

5 Conclusion

In this study, energy absorbers made of nested cylinders were investigated. After validation of the results obtained in LS-DYNA software and observation of high agreement between the experimental and numerical results, the collapse properties of the structures under quasi-static loading were investigated. The results obtained in the study showed that increasing the thickness of the wall or cylinder leads to an increase in collapse properties. So the amounts of Fm, Energy, CFE and Fa for absorbers which had more thickness were more than thin ones. Studies of force–displacement curves have shown that most of the peak forces in the force curve are due to the collapse or buckling of vertical walls.

In the studies performed on the absorbers of group C1, it was found that by increasing the wall thickness from 1 to 3, the stability of the maximum force increases. It was also found that higher wall thickness increases the probability of simultaneous collapse of both the upper and lower parts of the wall as compared to cylindrical thickness.

In the study of the absorbers of group C2, it was found that the force–displacement curves of these samples could be divided into three zones A, B and C and as the ratio of the cylinder thickness to the wall thickness increases, the difference between the peak force of zone B and the uniform force of zone A decreases.

The gravitational force diagrams of group C3 showed almost the same behavior. In most of these absorbers, with the exception of absorber C313, the absorber collapse in the initial 30 mm is related to the collapse of the innermost cylinder, after which the collapse continues with the buckling of one of the walls.

References

1. Davoodi MM, Sapuan SM, Yunus R (2008) Conceptual design of a polymer composite automotive bumper energy absorber. Mater Des 29(7):1447–1452
2. More KC, Patil GM, Belkhede AA (2020) Design and analysis of side door intrusion beam for automotive safety. Thin-Walled Struct 153:106788
3. Sun G, Guo X, Li S, Ruan D, Li Q (2020) Comparative study on aluminum/GFRP/CFRP tubes for oblique lateral crushing. Thin-Walled Struct 152:106420
4. Pan Z, Qiao F, Wang M, Wu Z, Ying Z (2021) A novel damage mechanism analysis of integrally braided CFRP and CFRP/ Aluminum hybrid composite tube subjected to transverse impact. Mater Des 206:109815
5. Wu Y, Sun L, Yang P, Fang J, Li W (2021) Energy absorption of additively manufactured functionally bi-graded thickness honeycombs subjected to axial loads. Thin-Walled Struct 164:107810
6. Rebelo HB, Lecompte D, Cismasiu C, Jonet A, Belkassem B, Maazoun A (2019) Experimental and numerical investigation on 3D printed PLA sacrificial honeycomb cladding. Int J Impact Eng 131:162–173
7. Usta F, Ertaş OF, Ataalp A, Türkmen HS, Kazancı Z, Scarpa F (2019) Impact behavior of triggered and non-triggered crash tubes with auxetic lattices. Multiscale Multidiscip Model Exp Des 2(2):119–127
8. Kucewicz M, Baranowski P, Małachowski J, Popławski A, Płatek P (2018) Modelling, and characterization of 3D printed cellular structures. Mater Des 142:177–189

9. Li S, Guo X, Li Q, Ruan D, Sun G (2020) On lateral compression of circular aluminium, CFRP and GFRP tubes. Compos Struct 232:111534
10. Alavi Nia A, Chahardoli S (2016) Optimizing the layout of nested three-tube structures in quasi-static axial collapse. Thin-Walled Struct 107:169–181
11. Wang Y, Zhai X, Liu S, Lu J, Zhou H (2020) Energy absorption performance of a new circular–triangular nested tube and its application as sacrificial cladding. Thin-Walled Struct 157:106992
12. Usta F, Türkmen HS (2019) Experimental and numerical investigation of impact behavior of nested tubes with and without honeycomb filler. Thin-Walled Struct 143:106256
13. Yang X, Ma J, Sun Y, Yang J (2019) An internally nested circular-elliptical tube system for energy absorption. Thin-Walled Struct 139:281–293
14. Xu B, Wang C, Xu W (2019) An efficient energy absorber based on fourfold-tube nested circular tube system. Thin-Walled Struct 137:143–150
15. Tran T (2018) A study on nested two-tube structures subjected to lateral crushing. Thin-Walled Struct 129:418–428
16. Baroutaji A, Gilchrist MD, Olabi AG (2016) Quasi-static, impact and energy absorption of internally nested tubes subjected to lateral loading. Thin-Walled Struct 98:337–350
17. Baroutaji A, Morris E, Olabi AG (2014) Quasi-static response and multi-objective crashworthiness optimization of oblong tube under lateral loading. Thin-Walled Struct 82:262–277
18. Baroutaji A, Gilchrist MD, Smyth D, Olabi AG (2015) Crush analysis and multi-objective optimization design for circular tube under quasi-static lateral loading. Thin-Walled Struct 86:121–131
19. Nia AA, Chahardoli S (2016) Mechanical behavior of nested multi-tubular structures under quasi-static axial load. Thin-Walled Struct 106:376–389
20. Alavi Nia A, Khodabakhsh H (2015) The effect of radial distance of concentric thin-walled tubes on their energy absorption capability under axial dynamic and quasi-static loading. Thin-Walled Struct 93:188–197
21. Elahi SA, Rouzegar J, Niknejad A, Assaee H (2017) Theoretical study of absorbed energy by empty and foam-filled composite tubes under lateral compression. Thin-Walled Struct 114:1–10
22. Chahardoli S, Akhavan Attar A, Ziaie M, Hossaeini Marashi SM (2022) Introducing new nested absorbers with square cross-sections and optimization of their performance using Response Surface Method under quasi-static loading, Proceedings of the Institution of Mechanical Engineers, Part L: Journal of Materials: Design and Applications, 14644207221075836
23. Chahardoli S, Alavi Nia A, Asadi M (2019) A parametric study of the mechanical behavior of nested multi tube structures under quasi-static loading. Arch Civil Mech Eng 19(4):943–957
24. Tang Z, Liu S, Zhang Z (2013) Analysis of energy absorption characteristics of cylindrical multi-cell columns. Thin-Walled Struct 62:75–84
25. Zhang X, Zhang H (2014) Axial crushing of circular multi-cell columns. Int J Impact Eng 65:110–125
26. ASTME8/E8M-09 (2009) Standard Test Methods for Tension Testing of Metallic Materials, ASTM International, West Conshohocken, PA, www.astm.org, ASTM2011.
27. Yin H, Wen G, Liu Z, Qing Q (2014) Crashworthiness optimization design for foam-filled multi-cell thin-walled structures. Thin-Walled Struct 75:8–17
28. Ahmad Z, Thambiratnam DP (2009) Crushing response of foam-filled conical tubes under quasi-static axial loading. Mater Des 30(7):2393–2403